Identifiability of parameters of three-phase oil relative permeability models under simultaneous water and gas (SWAG) injection

Ehsan Ranaee[1*], Leili Moghadasi[1], Fabio Inzoli[1], Monica Riva[2,3], Alberto Guadagnini[2,3]

[1]Dipartimento di Energia, Politecnico di Milano, Via Lambruschini 4, 20156 Milano, Italy

[2]Dipartimento di Ingegneria Civile e Ambientale, Politecnico di Milano, Piazza L. Da Vinci 32, 20133 Milano, Italy

[3]Department of Hydrology and Atmospheric Sciences, University of Arizona, Tucson, Arizona 85721, USA

* Corresponding author: Tel. +39 02 2399 3826. Fax. +39 02 2399 3913

E–mail address: ehsan.ranaee@polimi.it

Abstract

We assess the relative performance of a suite of selected models to interpret three-phase oil relative permeability data and provide a procedure to determine identifiability of the model parameters. We ground our analysis on observations of Steady-State two- and three-phase relative permeabilities we collect on a water-wet Sand-Pack sample through series of core-flooding experiments. Three-phase experiments are characterized by simultaneous injection of water and gas into the core sample initiated at irreducible water saturation, a scenario which is relevant for modern enhanced oil recovery techniques. The selected oil relative permeability models include classical and recent formulations and we consider their performance when (*i*) solely two-phase data are employed and/or (*ii*) two- and three-phase data are jointly used to render predictions of three-phase oil relative permeability, k_{ro}. We assess identifiability of model parameters through the Profile Likelihood (PL) technique. We rely on formal model discrimination criteria for a quantitative evaluation of the interpretive skill of each of the candidate models tested. We also evaluate the relative degree of likelihood associated with the competing models through a posterior probability weight and use Maximum Likelihood Bayesian model averaging to provide model-averaged estimate of k_{ro} and the associated uncertainty bounds. Results show that assessing identifiability of uncertain model parameters on the basis of the available dataset can provide valuable information about the quality of the parameter estimates and can reduce computational costs by selecting solely identifiable models among available candidates.

Keywords: relative permeability, parameter estimations, maximum likelihood, profile likelihood, identifiability analysis, model averaging.

1. Introduction

Proper characterization of flow under three-phase conditions is critical for a variety of field oriented industrial and environmental applications, including oil and gas production projects and their impacts on groundwater resources. Multiphase flow in porous media may potentially occur in hydrocarbon production scenarios and in the context of modern enhanced oil recovery (EOR) techniques based on simultaneous (or cyclic) injection of water and gas phases into an oil reservoir. In this framework, adequate characterization of relative permeabilities of fluid phases is of critical importance, since formulations based on analogues to Darcy's Law are routinely employed for the continuum-scale simulation of multiphase flow dynamics in porous and fractured media (e.g., Silpngarmlers et al., 2002 and references therein). A reliable characterization (either experimental or theoretical) of relative permeabilities, including a quantification of estimation uncertainty, enables us to assess the performance and efficiency of the reservoir production under the application of EOR techniques and the repercussions that these might have on the general subsurface flow circulation pattern, which is a key environmental concern in modern applications.

All these elements should be contrasted with the observation that experimental set-ups of three-phase flow systems are remarkably complex, costly, and time-consuming to design and operate. Due to a combination of these reasons, documentation and availability of three-phase relative permeability experiments is scarce (see, e.g., Oak, 1990; Blunt, 2000; Alizadeh and Piri, 2014a, b). A variety of empirical/semi-empirical models have been proposed for the characterization of three-phase relative permeabilities (e.g., Baker, 1988; Stone, 1970; Stone, 1973; Blunt, 2000; Spiteri and Juanes, 2004; Kianinejad and DiCarlo, 2016; Ranaee et al., 2016 and references therein). Ranaee et al. (2016) jointly employ Maximum Likelihood (ML) parameter estimation and model identification criteria to study the performance of a set of three-phase relative permeability models to interpret laboratory core-flooding datasets presented by Alizadeh

and Piri (2014b). The datasets analyzed include the dependence on phase saturation of two- and three-phase relative permeabilities collected under cyclic water alternating gas (WAG) injection scenarios. A main conclusion of Ranaee et al. (2016) is that the recent three-phase oil relative permeability model (termed Sigmoid model) proposed by Ranaee et al. (2015) appears to outperform the other tested models in interpreting the analyzed dataset. The need for additional testing against data-sets acquired under diverse conditions is also highlighted by the authors. This is precisely one of the objectives of the current study. We ground our analysis on the recent core-flooding data-sets presented by Moghadasi et al. (2016) and collected under simultaneous injection of water and gas (SWAG) phases. The data we analyze involve Steady-State two- and three-phase laboratory experiments performed on a quartz Sand-Pack sample.

An additional objective of our study is related to the assessment of the degree of reliability of the estimates of the parameters of calibrated relative permeability models. In this context, it is relevant to infer the reliability associated with such estimated model parameters on the basis of the amount and quality of available data (e.g., Neuman, 2003; Flassig et al., 2015) and to quantify the sensitivity of model responses to variations of uncertain model parameters (e.g., Tiedeman et al., 2004; Hou et al., 2015 and references therein). One then needs to assess the way parameter estimation uncertainty propagates onto bounds of uncertainty for model predictions (Kreutz et al., 2012 and references therein). We tackle these issues, including identifiability of model parameters, in the framework of a local sensitivity analysis (SA) performed on a selected suite of models. The challenges associated with the analysis are amplified by the type of flow process we examine and by the way the multi-phase flow physics are embedded (to various degrees) into each of the interpretive models.

Here we consider a collection of empirical models (see section 2.4) of three-phase oil relative permeability, k_{ro}, and: (*i*) rely on a Maximum Likelihood (ML) approach to compare the individual skill of each of these models to interpret k_{ro} data collected by Moghadasi et al. (2016) under

simultaneous injection of water and gas phases; (*ii*) quantify the uncertainties related to ML parameter estimates of each model; (*iii*) perform a comprehensive local sensitivity analysis for all model parameters; (*iv*) study the manifestation of possible structural and/or practical non-identifiability of model parameters through the use of the Profile Likelihood (PL) technique (Raue et al., 2009); and (*v*) illustrate the ability of ML Bayesian model averaging (MLBMA) approaches to interpret the analyzed dataset. We treat the models considered as a set of competing alternatives, rank them through model selection (or model discrimination) criteria and evaluate the posterior probability (or weight) associated with each of them. We assess the way the uncertainty linked to identifiable models parameters propagates to model outputs, i.e., k_{ro}, within a multimodel framework.

The work is organized as follows. Section 2.1 briefly illustrates the experimental core-flooding setup and the collected Steady-State two- and three-phase data of Moghadasi et al. (2016). The ML calibration procedure is briefly described in Section 2.2. Section 2.3 presents the Profile Likelihood (PL) technique for the assessment of identifiable model parameter(s). Section 2.4 illustrates the main features of the three-phase oil relative permeability models analyzed. Key results are presented in Section 3.

2. Materials and methods

2.1 Available dataset

The test bed we select comprises a three-phase core-flooding dataset collected on a water-wet Sand-Pack (Moghadasi et al., 2016, 2015a,b). Fig. 1 depicts a sketch of the setup employed in the experiments. The setup is designed as a closed-loop system. It comprises a core holder under a confinement pressure of 30 bars, an X-Ray apparatus for in-situ saturation detection and a three-phase separator. Experiments have been performed upon relying on the Steady-State method on a confined water-wet quartz Sand-Pack (length of 30 cm and cross-sectional diameter of 3.81 cm). The fluids used in the displacement experiments are water, isoparaffinic mineral oil and Nitrogen

gas (N_2). Water is tagged with an X-Ray absorbing chemical (*NaBr*) to allow for fluid saturation monitoring. The X-Ray apparatus includes a generator and a detector, a composite carbon core holder and a data acquisition system. The core sample is scanned from bottom to top, generating one-dimensional (1D) profiles of X-Ray attenuation. These data can be considered as representative of section-averaged saturations. The X-Ray beam employed to infer saturation of two-phase settings is generated by applying an electric potential of 55 kV and a current of 30 mA. To assess saturations in the three-phase experiments, we operated the X-Ray system at two diverse energy levels (E_i, i = 1, 2). We employed 55 kV-30 mA (E_1), and 90 kV-1 mA (E_2), following preliminary system calibrations. These values are kept constant during the experiments. The two streams of oil and water are re-injected from the separator to the core by dual piston syringe pumps. The gas is first conveyed through a humidification system and is then injected into the core by a pump. The gas discharged from the core is collected in the three-phase separator and is then released from the system through a gasometer (see Fig. 1). The humidification component is essentially formed by a cylinder containing the test oil and water and within which the gas is bubbled. The temperature in this component is about 40°C higher than room temperature. The procedure is designed to avoid drying of the core during gas injection. Gas flow rates are controlled by a mass-flow meter placed upstream of the humidification system. Two pressure transducers are employed to measure continuously the pressure drop across the core.

Fig. 1.

Two- and three-phase Steady-State (SS) laboratory experiments are performed by simultaneous injection of fluids into the core sample, according to the steps depicted in Fig. 2. The system state resulting from each of the steps described in the following is maintained for 24 hours to ensure attainment of equilibrium conditions. Before initiating the (two- or three-phase) experiments, the core sample is fully saturated with water. Absolute permeability of the core sample

to the water phase is determined by applying a sequence of diverse flow rates and employing Darcy's law (Step A in Figs. 2a, b). Oil is then injected to displace water. This drainage process takes place until no more water is eluted from the system. The (highest) value of oil relative permeability, $\overline{k}_{row}^{M}$, is then determined at such irreducible (connate) water saturation, $\overline{S}_{wc}$, condition (Step B in Figs. 2a, b).

Joint injection of the oil and water phases is performed for the two-phase setting by applying a total constant flow rate of 480 ml/h (corresponding to an average velocity of 90 ft/day, porosity of the core sample being equal to 0.37). The collection of experimental data is performed by increasing the water fractional flow rate while decreasing the oil fractional flow rate (Steps C-E in Fig. 2a). For a given fractional flow rate, measurements of fluid saturations and pressure drop (across the core sample) are taken at Steady-State (SS) conditions. Note that, as mentioned above, each step takes almost 24 hours to attain equilibrium. Residual oil saturation, $\overline{S}_{orw}$, is established at the end of the oil-water imbibition process, when no more oil is eluted from the core (Step F in Fig. 2a). A series of SS drainage experiments are then performed on the core sample, starting at $\overline{S}_{orw}$ and increasing oil and decreasing water fractional flow rates. The Steady-State oil-gas drainage process is also assessed through a similar experimental procedure by simultaneous injection of oil and gas (increasing gas and decreasing oil flow rates) into the core sample initiated at $\overline{S}_{wc}$.

The three-phase SS experiment is started at two-phase $\overline{S}_{wc}$ (in presence of oil, Step B in Fig. 2b) and is performed by simultaneous injections of water, oil and gas. The three-phase dataset includes oil relative permeabilities collected under an Increasing-Decreasing-Increasing saturation path (termed IDI, referring here to increasing water, decreasing oil and increasing gas fractional flow rates). Such an IDI path is obtained by systematically varying the fractional flow of water, gas and oil for a set of successive flow rate setting. Water and gas rates are increased accordingly. Note that a given experimental step is considered to be completed when the system attains equilibrium in

terms of pressure and fluid distributions (saturations). Two to four days are typically needed for each set of flow rates to achieve Steady-State. The last step of the experiments is performed through injection of only water and gas into the core sample (Step F in Fig. 2b). This experimental procedure can be considered as representative of typical reservoir conditions during primary oil production.

Saturation values are recorded during both two- and three-phase experiments by means of an in-situ X-Ray saturation monitoring technique. X-Ray scans of the rock sample are performed after each step for the assessment of saturation profiles. Relative permeabilities are finally calculated upon applying Darcy's law and are associated with the corresponding depth-averaged core saturations (see Moghadasi et al., 2015, 2016 for additional details).

Fig. 2.

Data of oil relative permeabilities observed from (*a*) two-phase oil-water, $\overline{k}_{row}$, and oil-gas, $\overline{k}_{rog}$, systems, and (*b*) three-phase, k_{ro}, experiments are depicted in Fig. 3 versus oil saturation. Results indicate a clear hysteretic behavior of $\overline{k}_{row}$, when switching from drainage, $\overline{k}^{D}_{row}$, to imbibition, $\overline{k}^{I}_{row}$, conditions. Since in oil-gas systems of water-wet conditions the two-phase relative permeability, $\overline{k}_{rog}$, of the porous medium to oil (the wetting phase) does not reveal hysteresis effects (e.g., Spiteri and Juanes, 2004) in Fig. 3 we depict only data collected during drainage experiments, $\overline{k}^{D}_{rog}$.

Fig. 3.

2.2 Maximum Likelihood model parameter estimation

This section briefly outlines the Maximum Likelihood (ML) framework employed to estimate model parameters and associated bounds of uncertainty in the context of the relative permeability models. We introduce the vector $\mathbf{Y}$, whose entries are n values of $Y_i = \log k_{ro,i}$ (with i = 1, …, n), $k_{ro,i}$ being relative oil permeability at oil saturation equal to $S_{o,i}$. Vector $\mathbf{Y}^*$ contains n available noisy measurements of Y_i, $Y_i^* = \log k_{ro,i}^*$. For a given model, a ML estimate, $\hat{\boldsymbol{\theta}}$, of vector, $\boldsymbol{\theta}$, whose entries are m model parameters, can be obtained through minimization of the negative log likelihood criterion, *NLL* (e.g., Carrera and Neuman, 1986)

$$NLL = \frac{J}{\sigma_Y^2} + n \ln(2\pi\sigma_Y^2); \qquad J = \sum_{i=1}^{n} \varepsilon_i^2; \qquad \varepsilon_i = Y_i - Y_i^* \tag{1}$$

where σ_Y^2 is the measurement error variance, J is the global residual between model predictions and observations, ε_i is the i-th entry of the prior measurement error vector, which is supposed to be zero-mean Gaussian, uncorrelated. The quantity σ_Y^2 is generally unknown and its ML estimate can be obtained as

$$\hat{\sigma}_Y^2 = \frac{J_{\min}}{n} \tag{2}$$

$J_{\min}$ being the minimum value of J, i.e., $J_{\min} = J\left(\hat{\boldsymbol{\theta}}\right)$. The covariance matrix, $\mathbf{Q}$, of the estimation error is approximated by its Cramer-Rao lower bound as

$$\mathbf{Q} = \hat{\sigma}_Y^2 \left(\mathbf{J}^T \mathbf{J}\right)^{-1} \tag{3}$$

where the superscript T denotes transpose and $\mathbf{J}$ is the $n \times m$ Jacobian matrix whose entries are the derivatives of the target variable, Y_i, with respect to model parameters evaluated at $\hat{\boldsymbol{\theta}}$. We minimize (1) through a gradient based method (e.g., Nocedal and Wright, 2006), as implemented in

Matlab® environment. The square root of a given diagonal term of $\mathbf{Q}$ yields the ML estimate of the estimation error of the corresponding model parameter, $\hat{\sigma}_{\theta_i}^{ML}$. This information can be employed to evaluate the upper, $\theta_{i\_U}^{ML}$, and lower, $\theta_{i\_L}^{ML}$, limits of the confidence intervals of each parameter estimate with a given significance level α as

$$\theta_{i\_U}^{ML} = \hat{\theta}_i + \sqrt{\chi_\alpha^2}\ \hat{\sigma}_{\theta_i}^{ML}; \qquad \theta_{i\_L}^{ML} = \hat{\theta}_i - \sqrt{\chi_\alpha^2}\hat{\sigma}_{\theta_i}^{ML} \tag{4}$$

χ_α^2 being the α-quantile of the χ^2 distribution with one degree of freedom. Confidence intervals, CIs, of parameter estimates can also been identified by introducing a threshold in the likelihood (i.e., the so called finite sample confidence intervals) as (Meeker and Escobar, 1995)

$$\left\{\theta_{i\_L}^{PL}, \theta_{i\_U}^{PL} \,|\, \frac{J(\theta_i) - J(\hat{\theta}_i)}{\sigma_Y^2} = \chi_\alpha^2\right\} \tag{5}$$

Note that CIs defined through (4) are symmetric around $\hat{\theta}_i$. Otherwise, CIs calculated on the basis of (5) can be strongly asymmetric around parameter estimates, as we illustrate in Section 3.

When N_M multiple models are considered to interpret a physical scenario of interest, one may minimize (1) for each candidate model. Once the parameters associated with each model are estimated, the N_M alternative formulations can be ranked by way of selection (or discrimination) criteria (e.g., Neuman, 2003; Ye et al., 2004, 2008; Haddad and Rahman, 2011; Neuman et al., 2012 and references therein). These include AIC_c (Hurvich and Tsai, 1989), BIC (Schwarz, 1978) and KIC (Kashyap, 1982), respectively defined as

$$AIC_c = NLL + 2m + \frac{2m(m+1)}{n-m-1} \tag{6}$$

$$BIC = NLL + m\ln n \tag{7}$$

$$KIC = NLL - m\ln(2\pi) - \ln|\mathbf{Q}| \tag{8}$$

Model discrimination criteria can also be employed to determine posterior model weight (for AIC_c) or posterior model probability (for *BIC* and *KIC*), $p(M_k \mid \mathbf{Y}^*)$, as (Ye et al., 2008)

$$p(M_k \mid \mathbf{Y}^*) = \frac{\exp\left(-\frac{1}{2}\Delta IC_k\right) p(M_k)}{\sum_{i=1}^{N_M} \exp\left(-\frac{1}{2}\Delta IC_i\right) p(M_i)} \tag{9}$$

Here, $\Delta IC_k = IC_k - IC_{\min}$, IC_k being a given model discrimination criterion (6)-(8); $IC_{\min}$ is the minimum value of IC_k across the N_M candidate models, and $p(M_k)$ is the prior probability of model M_k.

We also employ ML Bayesian Model Averaging (MLBMA) (Neuman, 2003; Ye et al., 2004; 2010; Tsai, 2010) to combine the predictive capabilities of the suite of models considered. Relative permeability values averaged across the model space and conditional to the available data, $E(\mathbf{Y} \mid \mathbf{Y}^*)$, can then be calculated by weighting each model through its posterior probability (Ye et al., 2010) as

$$E(\mathbf{Y} \mid \mathbf{Y}^*) = \sum_{k=1}^{N_M} E(\mathbf{Y} \mid \mathbf{Y}^*, M_k)\, p(M_k \mid \mathbf{Y}^*) \tag{10}$$

$E(\mathbf{Y} \mid \mathbf{Y}^*, M_k)$ being the posterior mean $\mathbf{Y}$ computed for model M_k. The mean permeability value (10) is then complemented by the associated variance

$$Var(\mathbf{Y} \mid \mathbf{Y}^*) = \sum_{k=1}^{N_M} Var(\mathbf{Y} \mid \mathbf{Y}^*, M_k)\, p(M_k \mid \mathbf{Y}^*) + \sum_{k=1}^{N_M} \left[E(\mathbf{Y} \mid \mathbf{Y}^*, M_k) - E(\mathbf{Y} \mid \mathbf{Y}^*)\right]^2 p(M_k \mid \mathbf{Y}^*) \tag{11}$$

$Var(\mathbf{Y} \mid \mathbf{Y}^*, M_k)$ being the posterior variance of $\mathbf{Y}$ associated with model M_k.

2.3 Model parameter identifiability

An important step in a model selection and calibration framework is the assessment of the identifiability of model parameters. Following Raue et al. (2011), depending on the available dataset and on the model structure, one can distinguish between (*i*) identifiability, (*ii*) practical non-identifiability and/or (*iii*) structural non-identifiability of model parameters. The identifiability analysis is performed on the basis of the global residual J given by (1). For illustration purposes, Fig. 4 depicts the ratio J/σ_Y^2 for a two-dimensional parameter space (θ_1, θ_2) and for three showcases respectively depicting identifiability (Fig. 4a), practical non-identifiability (Fig. 4b) and structural non-identifiability (Fig. 4c). Figures 4a-c also include the parameter estimate confidence intervals, CIs, as defined by (5). Parameter θ_i is identifiable if the minimum of (1) is unique and the area enclosed by the CI in the parameter space is finite and fully included in the parameter space (see, e.g., Fig. 4a, b). Finally, structural non-identifiability is related to the model structure, regardless of the quality and/or quantity of the data collected (Cobelli and DiStefano, 1980), and arises from a non-unique solution of minimization of (1) (see Fig. 4c).

Fig. 4.

We assess here identifiability of model parameter θ_i through its profile likelihood (PL), $\delta_{PL}(\theta_i)$, defined as (Raue et al., 2009)

$$\delta_{PL}(\theta_i) = \min_{\theta_{j\neq i}} \left[\frac{J(\theta_j)}{\sigma_Y^2} \right] \tag{12}$$

with $\sigma_Y^2 = \hat{\sigma}_Y^2$ i.e. $\delta_{PL}(\theta_i)$ is calculated by minimizing J from (1) with respect to all model parameters except θ_i. Fig. 4d depicts the PL of the identifiable parameter θ_1. In this case $\delta_{PL}(\theta_1)$ displays a unique minimum (at the ML estimate of θ_1, $\hat{\theta}_1$) and increases for both increasing and decreasing values of θ_1 around $\hat{\theta}_1$, resulting in a region of finite extent and fully included in the parameter space explored for model calibration. In the case of practical non-identifiability (see Fig. 4e), $\delta_{PL}(\theta_i)$ displays a unique minimum value, but the lower or/and upper limits of the CIs, i.e. $\theta_{i\_L}^{PL}$ or $\theta_{i\_U}^{PL}$ in (5), reaches the assigned bounds of the parameter space. Structural non-identifiability, as illustrated in Fig. 4f, results in a flat behavior of $\delta_{PL}(\theta_i)$ within the parameter range of variability.

2.4 Three-phase oil relative permeability models

A variety of empirical and semi-empirical formulations is available and is routinely used for the characterization of three-phase relative permeabilities. Each model may be associated with a set of parameters which can be estimated by model calibration through experiments, i.e., available saturation-relative permeability data. Here, we analyze the behavior of four models, which we select amongst classical and relatively recent formulations, in terms of their skill to characterize three-phase oil relative permeability, k_{ro}, data. An extensive analysis of k_{ro} available models has been recently presented by Ranaee et al. (2016). With respect to these authors, here we do not consider the models introduced by Delshad and Pope (1989) and Lomeland and Ebeltoft (2013) since they require the evaluation of a large number of parameters ($m \geq 5$) which cannot be estimated when, as is often the case, the amount of available k_{ro} data, n, is limited. Note that $n = 6$ for the analyzed data set (see also Fig. 3). The main features of the tested models are briefly described in the following.

2.4.1 Stone model (*M1*)

Stone (1970) proposed an empirical model to evaluate k_{ro}, when the maximum value of oil relative permeability in an oil-water system at irreducible water saturation (i.e., in the presence of connate water), $\bar{k}_{row}^{M}$, is set to unity. Here, we consider the modified version proposed by Aziz and Settari (1979)

$$k_{ro} = \frac{\bar{k}_{row}^{I}\bar{k}_{rog}^{D}}{\bar{k}_{row}^{M}} \frac{S_o^N}{\left(1-S_w^N\right)\left(1-S_g^N\right)} \tag{13}$$

where $\bar{k}_{rog}^{D}$ and $\bar{k}_{row}^{I}$ are relative permeabilities of the oil phase observed in two-phase systems, respectively during drainage of gas (in the presence of connate water saturation, $\bar{S}_{wc}$) and imbibition of water; S_w^N, S_o^N and S_g^N are rescaled saturations evaluated as

$$S_w^N = \frac{S_w - \bar{S}_{wc}}{1-\bar{S}_{wc}-S_{or}}; \quad S_o^N = \frac{S_o - S_{or}}{1-\bar{S}_{wc}-S_{or}}; \quad S_g^N = \frac{S_g}{1-\bar{S}_{wc}-S_{or}} \tag{14}$$

S_w, S_o and S_g respectively being water, oil and gas saturations in a three-phase environment. Note that $\bar{k}_{row}^{I}$ and $\bar{k}_{rog}^{D}$ in (13) are evaluated at oil saturation respectively equal to $(1-S_w)$ and $(1-S_g-\bar{S}_{wc})$. When only two-phase data are available, the residual oil saturation, S_{or} is typically calculated as (Fayers and Matthews, 1984)

$$S_{or} = a\bar{S}_{row} + (1-a)\bar{S}_{rog} \qquad \text{with} \quad a = 1 - \frac{S_g}{1-\bar{S}_{wc}-\bar{S}_{rog}} \tag{15}$$

Here, $\bar{S}_{row}$ and $\bar{S}_{rog}$ represent two-phase residual oil saturations in water-oil and gas-oil systems, respectively. In the presence of three-phase relative permeability data one may consider S_{or} as a model parameter to be estimated through ML as described in Section 2.1. The model parameter vector has only one entry in this case, i.e., $\theta_1 = S_{or}$. The estimation variance of θ_1, i.e., $\hat{\sigma}_{\theta_1}^2$ can readily be evaluated analytically as

$$\hat{\sigma}_{\theta_1}^2 = 5.3\left(1-\overline{S}_{wc}-S_{or}\right)^2 \hat{\sigma}_Y^2 \left[\sum_{i=1}^{n}\left[\frac{-1+\overline{S}_{wc}+S_{o,i}}{S_{o,i}-S_{or}}+\frac{S_{w,i}-\overline{S}_{wc}}{1-S_{or}-S_{w,i}}+\frac{S_{g,i}}{1-\overline{S}_{wc}-S_{or}-S_{g,i}}\right]^2\right]^{-1} \quad (16)$$

2.4.2 Baker model (M_2)

Baker (1998) proposed the use of a saturation-weighted interpolation model between (two-phase) oil/water and oil/gas data to evaluate three-phase oil relative permeability. Here, we consider the following modified version of the Baker model, as introduced by Pejic and Maini (2003)

$$k_{ro} = \frac{S_w^N \overline{k}_{row}^I + S_g^N \overline{k}_{rog}^D}{S_w^N + S_g^N} \quad (17)$$

where

$$S_w^N = \frac{S_w - \overline{S}_{wc}}{1-\overline{S}_{wc}-S_{or}}; \qquad S_g^N = \frac{S_g - \overline{S}_{gt}}{1-\overline{S}_{wc}-\overline{S}_{gt}-S_{or}} \quad (18)$$

$\overline{S}_{gt}$ being the two-phase trapped gas saturation. All remaining symbols have already been defined. When three-phase data are not available, S_{or} is usually estimated by (15) while $\overline{S}_{gt}$ is set equal to zero (Spitteri and Juanes, 2004). In the presence of three-phase data, the two model parameters, $\theta_1 = S_{or}$ and $\theta_2 = \overline{S}_{gt}$, can be estimated via ML. The entries of matrix **Q** in (3) are then given by

$$Q_{1,1} = \hat{\sigma}_{\theta_1}^2 = \frac{\hat{\sigma}_Y^2}{\left\|\mathbf{J}^T\mathbf{J}\right\|}\sum_{i=1}^{n}\left(\frac{\partial Y_i}{\partial \theta_2}\right)^2; \quad Q_{2,2} = \hat{\sigma}_{\theta_2}^2 = \frac{\hat{\sigma}_Y^2}{\left\|\mathbf{J}^T\mathbf{J}\right\|}\sum_{i=1}^{n}\left(\frac{\partial Y_i}{\partial \theta_1}\right)^2; \quad Q_{1,2} = Q_{2,1} = -\frac{\hat{\sigma}_Y^2}{\left\|\mathbf{J}^T\mathbf{J}\right\|}\sum_{i=1}^{n}\frac{\partial Y_i}{\partial \theta_1}\frac{\partial Y_i}{\partial \theta_2} \quad (19)$$

where $Y_i = \log k_{ro,i}$ and

$$\left\|\mathbf{J}^T\mathbf{J}\right\| = \sum_{i=1}^{n}\left(\frac{\partial Y_i}{\partial \theta_1}\right)^2 \sum_{i=1}^{n}\left(\frac{\partial Y_i}{\partial \theta_2}\right)^2 - \left[\sum_{i=1}^{n}\frac{\partial Y_i}{\partial \theta_1}\frac{\partial Y_i}{\partial \theta_2}\right]^2 \quad (20)$$

2.4.3 Model M_3 (Du et al. 2004)

Du et al. (2004) introduced the following model for three phase oil relative permeability

$$k_{ro} = \frac{\left(S_w - \overline{S}_{wc}\right)\left(S_w + AS_g\right)}{\left(S_w + S_g - \overline{S}_{wc}\right)} \overline{k}_{row}^{I} + \frac{S_g\left(B\left(S_w - \overline{S}_{wc}\right) + S_g\right)}{\left(S_w + S_g - \overline{S}_{wc}\right)} \overline{k}_{rog}^{D} \tag{21}$$

According to Du et al. (2004), the parameters A and B are typically set to 0.9 and 0.95, respectively, in the absence of three-phase data. When three-phase data are available, the two model parameters $\theta_1 = A$ and $\theta_2 = B$ can be estimated via ML and entries of matrix **Q** are given by (19) - (20).

2.4.4 Sigmoid model (M_4)

According to Ranaee et al. (2015) k_{ro} during gas, $k_{ro} = k_{ro}^{G}$, and water, $k_{ro} = k_{ro}^{W}$, injection can be estimated as

$$k_{ro}^{G} = \max(k_{ro}^{S}, \overline{k}_{rog}^{D}); \qquad k_{ro}^{W} = \frac{\left(S_w - \overline{S}_{wc}\right)k_{ro}^{S} + \left(S_g - \overline{S}_{gt}\right)\overline{k}_{rog}^{D}}{\left(S_w - \overline{S}_{wc}\right) + \left(S_g - \overline{S}_{gt}\right)} \tag{22}$$

where k_{ro}^{S} is given by

$$k_{ro}^{S} = \frac{\overline{k}_{row}^{M} S_o}{\overline{S}_{ow}^{M} + \exp\left[\lambda - \beta\left(\frac{S_o}{\overline{S}_{ow}^{M}}\right)^{\overline{S}_{ow}^{M}}\right]} \tag{23}$$

Here, $\overline{S}_{ow}^{M}$ is the largest oil saturation observed in a two-phase (oil-water) system in the presence of connate water. SWAG experiments analyzed in this work and detailed in Section 2.1 are characterized by gas-oil mobility ratio significantly larger (about 50 – 100 times) than the water-oil mobility ratio. A high mobility ratio causes poor displacement and volumetric sweep efficiency (e.g., Lyons and Plisga, 2005; Suicmez et al., 2007; Sohrabi et al., 2008). Therefore, water has been

considered as the main displacing phase in our SWAG experiments. Accordingly, we set $k_{ro} = k_{ro}^{W}$ in (22).

Parameters λ and β in (22) can be evaluated solely on the basis of two-phase (oil-gas and oil-water) data (Ranaee et al., 2015) as

$$\lambda = \ln\left[\frac{\overline{k}_{row}^{M} S_o^{inf}}{k_{ro}^{inf}} - \overline{S}_{ow}^{M}\right] + \beta\left(\frac{S_o^{inf}}{\overline{S}_{ow}^{M}}\right)^{\overline{S}_{ow}^{M}}; \qquad \beta = \frac{1}{\overline{S}_{ow}^{M}}\left(\frac{m_{inf} S_o^{inf}}{k_{ro}^{inf}} - 1\right)\left(1 - \frac{\overline{S}_{ow}^{M} k_{ro}^{inf}}{\overline{k}_{row}^{M} S_o^{inf}}\right)^{-1}\left(\frac{S_o^{inf}}{\overline{S}_{ow}^{M}}\right)^{-\overline{S}_{ow}^{M}} \tag{24}$$

with

$$S_o^{inf} = \overline{S}_{row} + \frac{\overline{S}_{ow}^{M} - \overline{S}_{row}}{2}; \qquad k_{ro}^{inf} = \overline{k}_{row}^{I}\left(S_o^{inf}\right); \qquad m_{inf} = \left.\frac{\partial \overline{k}_{row}^{I}}{\partial S_o}\right|_{S_o^{inf}} \tag{25}$$

i.e., m_{inf} is the slope of $\overline{k}_{row}^{I}$ at S_o^{inf}. When three-phase data are available, parameters $\theta_1 = \lambda$ and $\theta_2 = \beta$ can be estimated within a ML framework and entries of matrix **Q** are given by (19) - (20).

3. Results and discussion

Fig. 5 depicts three-phase oil relative permeability estimates evaluated relying solely on two-phase data (Fig. 5a) and calibrating model parameters by ML making use of two- and three-phase data (Fig. 5b). Available three-phase oil relative permeability data associated with the considered SWAG experiment are also reported. Visual inspection of Fig. 5a and Fig. 5b suggests that models *M2* and *M4* yield quite reasonable estimates of k_{ro} through the entire range of saturations. Model *M1* tends to overestimate k_{ro} for high oil saturations, while *M3* underestimates k_{ro} for all saturation values. Model predictions tend to improve when parameters are estimated through ML on the basis of three-phase data. These results are further supported by Table 1, which lists values of (*i*) Mean Square Difference *MSD* = *J* / *n*, where *J* is given by (1) and represents the discrepancy between k_{ro} (evaluated on the basis of only two-phase data) and three-phase data; (*ii*) ML model parameter

estimates, $\hat{\theta}_i$, evaluated by minimizing (1) and making use of the available three-phase k_{ro} data; (*iii*) ML estimates of measurement error variance, $\hat{\sigma}_Y^2$ (2); and (*iv*) ML estimates of the estimation error of each parameter quantified by $\hat{\sigma}_{\theta_i}^{ML}$ and evaluated as described in Section 2.2. Note that (*i*) ML calibration on the basis of three-phase data does not lead to an improvement of the results associated with model *M2*, i.e., *MSD* = $\hat{\sigma}_Y^2$, and (*ii*) *MSD* evaluated with model *M4* is smaller than $\hat{\sigma}_Y^2$ computed for *M2* and *M3*. This observation implies that *M4* is conducive to estimates of k_{ro} of higher quality than those rendered by *M2* and *M3*, even in cases where three-phase data are included in *M2* and *M3* and are not considered in *M4*.

Table 1

Fig. 5.

We then analyze the entries of the covariance matrix **Q** (3) associated with each of the tested models. Fig. 6a depicts normalized uncertainty intervals, quantified by $(\hat{\theta}_i + \hat{\sigma}_{\theta_i}^{ML})/\hat{\theta}_i$, for all ML model parameter estimates. We can observe that ML estimates of the parameters of model *M4* are associated with the smallest (normalized) uncertainty, estimates of model *M2* parameters being linked to the largest estimation uncertainties.

We also perform a local sensitivity analysis to address relative sensitivity of parameter estimates to model responses. Fig. 6b illustrates normalized model sensitivities calculated at the ML estimate, $\hat{\theta}_i$, for each of the available oil relative permeability data, $k_{ro,i}^*$. These results show that ML-based model parameter sensitivities are virtually zero for the largest $k_{ro,i}^*$ values. This result

might be related to the selected structure of the objective function (1), which is formulated in terms of the logarithm of model responses and available observations. It is clear that the parameters associated with the sigmoid model M_4 are associated with the highest sensitivity, for small to intermediate oil saturation values.

Fig. 6.

We now employ the PL technique described in Section 2.3 to investigate identifiability of model uncertain parameters. Fig. 7 (black continuous curve) depicts the difference $\delta_{PL}(\theta_i) - \delta_{PL}(\hat{\theta}_i)$ evaluated making use of (12) for all model parameters (i.e., S_{or} for M_1; S_{or}, and $\bar{S}_{gt}$ for M_2; A, and B for M_3; and λ, and β for M_4). The horizontal dashed lines represent the thresholds χ^2_α with significance level α = 0.317 (blue dashed lines) and 0.05 (green dashed lines). The intercept of these lines with the curve $\delta_{PL}(\theta_i) - \delta_{PL}(\hat{\theta}_i)$ yields the lower, $\theta^{PL}_{i\_L}$, and upper, $\theta^{PL}_{i\_U}$, bounds of the finite sample 68% (for α = 0.317) and 95% (for α = 0.05) Cis, as defined by (5). As additional term of comparison, Fig. 7 also depicts the ML upper, $\theta^{ML}_{i\_U}$, and lower, $\theta^{ML}_{i\_L}$, bounds of the CIs evaluated via (4) for α = 0.317 (vertical red dashed line) and α = 0.05 (vertical red continuous line). Fig. 7 clearly shows that ML confidence intervals are significantly narrower than finite sample CIs. The latter are characterized by a strong positive asymmetry around $\hat{\theta}_i$.

Fig. 7.

The results of Fig. 7a are indicative of practical non-identifiability of the model M_1 parameter (S_{or}), the profile likelihood displaying similar features of Fig. 4e. This finding suggests that the

amount and/or quality of the available experimental data do not contain enough information to yield a reliable estimate of S_{or} for the Stone model. Regarding model M_2, the profile likelihood suggests structural non-identifiability for parameter S_{or} (see Fig. 7b) and practical non-identifiability for parameter $\overline{S}_{gt}$ (see Fig. 7c). Otherwise, PL analyses of models M_3 and M_4 reveal identifiability of the model parameters, albeit with diverse degrees of uncertainty. Table 2 lists the ML and sample 68% and 95% CIs bounds for models (M_3 and M_4) with identifiable parameters. ML and sample bounds of CIs are notably different, their percentage difference ranging from 40% to more than 300%. As already noticed, sample CIs are (generally) not symmetric around $\hat{\theta}_i$, as otherwise observed for the ML CIs. This feature is typically considered as a shortcoming of ML results, based on (4), especially for models exhibiting a highly nonlinear behavior as a function of the uncertain parameters (e.g., Joshi et al., 2006 and references therein). The relative extension of the CIs, as quantified by $\left(\theta^X_{i\_U} - \theta^X_{i\_L}\right) / \hat{\theta}_i$ (with $X = ML$ or PL), is generally smaller for M_4 than M_3.

Table 2

Fig. 8a depicts *NLL* (1) and model selection criteria (6)-(8) evaluated for all tested models. We observe that three out of four criteria favor the use of model M_4 for the interpretation of the available three-phase k_{ro} data. These results are in agreement with our previous findings (see Ranaee et al., 2016) related to different injection scenarios and characteristics of the fluids and core samples than the one here considered. Fig. 8b depicts the posterior model weight (for AIC_c) and probability (for *BIC* and *KIC*), $p\left(M_k \mid \mathbf{Y}^*\right)$, for each candidate model. We assign an equal prior probability to each candidate model, i.e., $p\left(M_k\right) = 1 / N_M$ (k = 1,..., 4), in our analysis since prior information is not available. The highest posterior probability/weight is always assigned to model M_4, with the only exception of the results associated with the AIC_c (6) that prefer M_1. Note that AIC_c

and *BIC* tend to favor models solely on the basis of *NLL*, number of observations and number of parameters. Otherwise, *KIC* (8) tends to favor models with relatively small expected information content per observation (e.g., Hernandez et al., 2006; Ye et al., 2008; Riva et al., 2011). As such, *KIC* assigns a non-negligible posterior probability to model M_2, consistent with the associated values of the entries of **Q**, resulting in a relatively high uncertainty of parameter estimates (see also Fig. 6a). Our analysis is complemented by Fig. 8c, which depicts posterior probability/weight results obtained solely on the basis of models M_3 and M_4, the parameters of models M_1 and M_2 being associated with structural/practical non-identifiability, as discussed above. In this case, our results unequivocally reveal that model M_4 is always associated with a posterior model weight/probability which exceeds 90%.

Fig. 8.

Maximum Likelihood BMA is finally employed to provide a multi-model estimate of oil relative permeability via (9)-(11). Fig. 9 depicts scatterplots of MLBMA estimates versus observations of $Y^* = \log k_{ro}^*$ when replacing *IC* in (9)-(11) with (a) *NLL*, (b) AIC_c, (c) *BIC* and (d) *KIC*. We include results of MLBMA estimates obtained by considering all candidate models tested (denoted as $E\left(\mathbf{Y} \mid \mathbf{Y}^*\right)$ in Fig. 9) as well as those based solely on models M_3 and M_4, whose parameters are not affected by non-identifiability issues (denoted as $E\left(\tilde{\mathbf{Y}} \mid \mathbf{Y}^*\right)$ in the figure). Fig. 9 also depicts intervals of width $E\left(\mathbf{Y} \mid \mathbf{Y}^*\right) \pm \sqrt{Var\left(\mathbf{Y} \mid \mathbf{Y}^*\right)}$ as an additional term of comparison to characterize the uncertainties associated with MLBMA estimates. Corresponding $E\left(\tilde{\mathbf{Y}} \mid \mathbf{Y}^*\right) \pm \sqrt{Var\left(\tilde{\mathbf{Y}} \mid \mathbf{Y}^*\right)}$ bounds of uncertainties are included when considering MLBMA limited to models M_3 and M_4.

Generally, estimates of $\log k_{ro}^{*}$ and associated uncertainties computed on the basis of all tested models and solely on *M3* and *M4* are very similar. This indicates a very limited effect of the models with embedded non-identifiable parameters to improve predictions, a finding which is also in line with the small posterior probability associated with these latter models. These results clearly highlight the possibility of reducing candidate models to predict k_{ro} only to the identifiable ones, which can reduce computational costs of implementing the averaged model.

Fig. 9.

4. Concluding remarks

We analyze the performance of a suite of classical (Stone, 1970; Baker, 1988) and recent (Du et al., 2004; Ranaee et al., 2015) three-phase oil relative permeability models to reproduce recently published core-flooding dataset collected on a water-wet Sand-Pack. Three-phase experiments are characterized by simultaneous injection of water and gas (SWAG) into a core sample initiated at irreducible water saturation, a scenario which is relevant for modern enhanced oil recovery techniques. Our work leads to the following key conclusions.

1. The application of the Profile Likelihood (PL) technique seems to allow detecting both structural and practical identifiability of uncertain model parameter(s). Parameters related to classical and wide spread models, such as the Stone (1970) and Baker (1988) models, have been shown to be non-identifiable through the set of experiments analyzed in this work. This result raises serious doubts on the predictive capabilities of such classical formulations under SWAG conditions.
2. The use of three-phase data leads to significant improvement of model predictability only for models linked to identifiable parameters, e.g., *M3* (Du et al., 2004) and *M4* (Ranaee et al., 2016) in this study. Therefore, it is always recommended to perform a PL analysis before a

model calibration step. Such an analysis can reduce computational costs by embedding in the model calibration process solely identifiable models, as driven by the available dataset.

3. Maximum Likelihood (ML) confidence intervals, CIs, of parameter estimates are narrower than their counterparts evaluated on the basis of PL (i.e., finite sample CIs). This observation can lead to an over-reliance on the ML parameter estimates.
4. Considering models associated with identifiable parameters (i.e., M_3 and M_4), model selection criteria favor the use of M_4 for the interpretation of the available three-phase oil relative permeability data. Our results reveal that M_4 is associated with a posterior weight/probability which exceeds 90%.

Acknowledgments

Authors are grateful for the partial financial support from Eni SpA.

References

Alizadeh, A. H. and Piri, M., 2014a. Three-phase Flow in Porous Media: A Review of Experimental Studies on Relative Permeability. Reviews of Geophysics, 52:468-521. doi:10.1002/2013RG000433.

Alizadeh, A. H. and Piri M., 2014b. The Effect of Saturation History on Three–Phase Relative Permeability: An Experimental Study. Water Resources Research, 50: 1636-1664. doi:10.1002/2013WR014914.

Aziz, K. and Settari, A., 1979. Petroleum Reservoir Simulation. Applied Science Publishers, London.

Baker, L. E., 1998. Three-Phase Relative Permeability Correlations. SPE Enhanced Oil Recovery Symposium, Tulsa, Oklahoma. doi: 10.2118/17369-MS.

Blunt, M. J., 2000. An Empirical Model for Three-Phase Relative Permeability. SPE Journal, 5:435-445. doi:10.2118/67950-PA.

Carrera, J. and Neuman, S. P., 1986. Estimation of Aquifer Parameters under Transient and Steady State Conditions: 1. Maximum Likelihood Method in Cooperating Prior Information. Water Resources Research, 22(2):199-210. doi:10.1029/WR022i002p00199.

Cobelli, C. and DiStefano, J. J., 1980. Parameter and Structural Identifiability Concepts and Ambiguities: A Critical Review and Analysis. American Journal of Physiology-Regulatory, Integrative and Comparative Physiology, 239(1):7-24.

Delshad, M. and Pope, G. A., 1989. Comparison of the Three-Phase Oil Relative Permeability Models. Transport in Porous Media, 4:59-83. doi:10.1007/BF00134742.

Du, Y., Bolaji, O. B. and Li, D., 2004. Literature Review on Methods to Obtain Relative Permeability Aata. 5th conference and exposition on petroleum geophysics, Hyderabad India, 15-17 January.

Fayers, F. J. and Matthews, J. D., 1984. Evaluation of Normalized Stone's Methods for Estimating Three-Phase Relative Permeabilities. SPE Journal, 24(02):224-232. doi:10.2118/11277-PA

Flassig, R. J., Migal, I., Van. Der Zalm E., Rihko-Struckmann, L. and Sundmacher, K., 2015. Rational Selection of Experimental Readout and Intervention Sites for Reducing Uncertainties in Computational Model Predictions. BMC bioinformatics, 16:16-13. doi:10.1186/s12859-014-0436-5.

Hernandez. A. F., Neuman, S. P., Guadagnini, A. and Carrera, J., 2006. Inverse Stochastic Moment Analysis of Steady State Flow in Randomly Heterogeneous Media. Water Resources Research, 42(5):W05425. doi:10.1029/2005WR004449.

Hurvich, C. M. and Tsai, C. L., 1989. Regression and Time Series Model Selection in Small Samples. Biometrika, 76:297-307.

Kashyap, R. L., 1982. Optimal Choice of Ar and Ma Parts in Autoregressive Moving Average Models. IEEE Transactions on Pattern Analysis and Machine Intelligence, 4(2): 99-104.

Kianinejad, A. and DiCarlo, D. A., 2016. Three-Phase Oil Relative Permeability in Water-Wet Media: A Comprehensive Study. Transp. Porous Med. 112(3) 665-687. doi:10.1007/s11242-016-0669-z.

Haddad, K. and Rahman, A., 2011. Selection of the Best Fit Flood Frequency Distribution and Parameter Estimation Procedure: A Case Study for Tasmania in Australia. Stochastic Environ Res Risk Assess, 25(3):415-428. doi:10.1007/s00477-010-0412-1.

Hou, T., Zhu, Y., Lü, H., Sudicky, E., Yu, Z. and Ouyang, F., 2015. Parameter Sensitivity Analysis and Optimization of Noah Land Surface Model with Field Measurements from Huaihe River Basin, China. Stochastic Environ Res Risk Assess, 29(5):1383-1401. doi:10.1007/s00477-015-1033-5.

Joshi, M., Seidel-Morgenstern, A. and Kremling, A., 2006. Exploiting the Bootstrap Method for Quantifying Parameter Confidence Intervals in Dynamical Systems. Metabolic engineering, 8(5):447-455. doi:10.1016/j.ymben.2006.04.003.

Kreutz, C., Raue, A. and Timmer, J., 2012. Likelihood based Observability Analysis and Confidence Intervals for Predictions of Dynamic Models. BMC Systems Biology, 6(1):120.

Lyons, W. C. and Plisga, G. J., 2005. Standard Handbook of Petroleum and Natural Gas Engineering (Second edition). Burlington, MA: Elsevier Inc.

Lomeland, F. and Ebeltoft, E., 2013. Versatile Three-Phase Correlations for Relative Permeability and Capillary Pressure. International Symposium of the Society of Core Analysts, Napa Valley, California, USA, 16-19 September.

Meeker, W. and Escobar, L., 1995. Teaching about Approximate Confidence Regions Based on Maximum Likelihood Estimation. The American Statistician, 49(1):48-53. doi:10.2307/2684811

Moghadasi, L., Guadagnini, A., Inzoli, F., Bartosek, M. and Renna, D., 2016. Characterization of Two- and Three-Phase Relative Permeability of Water-Wet Porous Media through X-Ray Saturation Measurements. Journal of Petroleum Science and Engineering, 138:1-15. doi:10.1016/j.petrol.2016.05.031.

Moghadasi, L., Guadagnini, A., Inzoli, F. and Bartosek, M., 2015a. Interpretation of Two-Phase Relative Permeability Curves through Multiple Formulations and Model Quality Criteria. Journal of Petroleum Science and Engineering. 135: 738-749. doi:10.1016/j.petrol.2015.10.027.

Moghadasi, L., Guadagnini, A., Inzoli, F., Bartosek, M., Renna, D and Colapietro, D., 2015b. Laboratory-scale Investigation of Two-phase Relative Permeability. Procedia Environmental Sciences, 25: 166-174.

Neuman, S. P., 2003. Maximum Likelihood Bayesian Averaging of Uncertain Model Predictions. Stochastic Environmental Research and Risk Assessment, 17(5):291-305. doi:10.1007/s00477-003-0151-7.

Neuman, S. P., Xue, L., Ye, M. and Lu, D., 2012. Bayesian Analysis of Data-Worth Considering Model and Parameter Uncertainties. Advances in Water Resources, 36:75-85. doi:10.1016/j.advwatres.2011.02.007.

Nocedal, J. and Wright, S. J., 2006. Numerical Optimization. 2nd Ed Springer Verlag.

Oak, M. J., 1990. Three-Phase Relative Permeability of Water-Wet Berea. 7th SPE/DOE Enhanced Oil Recovery Symposium, Tulsa, Oklahoma, 22-25 April. doi:10.2118/20183-MS.

Pejic, D. and Maini, B. B., 2003. Three-Phase Relative Permeability of Petroleum Reservoirs. SPE 81021, SPE Latin American and Caribbean Petroleum Engineering Conference, Trinidad, 27-30 April. doi:10.2118/81021-MS.

Ranaee, E., Riva, M., Porta, G. M. and Guadagnini, A., 2016. Comparative Assessment of Three-Phase Oil Relative Permeability Models. Water Resources Research, 52(7):5341-5356. doi:10.1002/2016WR018872.

Ranaee, E., Porta, G. M., Riva, M., Blunt, M. J. and Guadagnini, A., 2015. Prediction of Three-Phase Oil Relative Permeability through a Sigmoid-Based Model. Journal of Petroleum Science and Engineering, 126:190-200. doi:10.1016/j.petrol.2014.11.034.

Raue, A., Kreutz, C., Maiwald, T., Bachmann, J., Schilling, M., Klingmuller, U. and Timmer, J., 2009. Structural and Practical Identifiability Analysis of Partially Observed Dynamical Models by Exploiting the Profile Likelihood. Bioinformatics, 25(15):1923-1929. doi: 10.1093/bioinformatics/btp358.

Raue, A., Kreutz, C., Maiwald, T., Klingmüller, U. and Timmer, J., 2011. Addressing Parameter Identifiability by Model-Based Experimentation. IET systems biology, 5(2):120-30. doi:10.1049/iet-syb.2010.0061.

Riva, M., Panzeri, M., Guadagnini, A. and Neuman, S. P., 2011. Role of Model Selection Criteria in Geostatistical Inverse Estimation of Statistical Data- and Model-Parameters. Water Resources Research, 47(7):W07502. doi:10.1029/2011WR010480.

Schwarz, G. E., 1978. Estimating the Dimension of a Model. Annals of Statistics, 6(2):461-464.

Silpngarmlers, N., Guler, B., Ertekin, T. and Grader, A. S., 2002. Development and Testing of Two-Phase Relative Permeability Predictors Using Artificial Neural Networks. SPE Journal, 7(03):299-308. doi:10.2118/79547-PA.

Sohrabi, M., Danesh, A. and Jamiolahmady, M., 2008. Visualisation of Residual Oil Recovery by Near-Miscible Gas and SWAG Injection Using High-Pressure Micromodels. Transport in Porous Media, 74:239-257. doi:10.1007/s11242-007-9193-5

Spiteri, E. J., and Juanes, R., 2004. Impact of Relative Permeability Hysteresis on the Numerical Simulation of WAG Injection. Journal of Petroleum Science and Engineering, 50:115-139. doi:10.1016/j.petrol.2005.09.004.

Stone, H. L., 1973. Estimation of Three-phase Relative Permeability and Residual oil Data. J. Can. Petrol. Technol. 12, 53–61. doi:10.2118/73-04-06.

Stone, H. L., 1970. Probability Model for Estimation of Three-Phase Relative Permeability. Journal of Petroleum Technology, 22:214-218.

Suicmez, V. S., Piri, M. and Blunt, M. J., 2007. Pore-Scale Simulation of Water Alternate Gas Injection. Transport in Porous Media, 66:259-286. doi:10.1007/s11242-006-0017-9.

Tsai, F. T. C., 2010. Bayesian Model Averaging Assessment on Groundwater Management under Model Structure Uncertainty. Stochastic Environmental Research and Risk Assessment, 24(6):1436-3259. doi:10.1007/s00477-010-0382-3.

Tiedeman, C. R., Ely, D. M., Hill, M. C. and O'Brien, G. M., 2004. A Method for Evaluating the Importance of System State Observations to Model Predictions, with Application to the Death Valley Regional Groundwater Flow System. Water Resources Research, 40(12)W12411. doi: 10.1029/2004WR003313.

Ye, M., Neuman, S. P. and Meyer, P. D., 2004. Maximum Likelihood Bayesian Averaging of Apatial Variability Models in Unsaturated Fractured Tuff. Water Resources Research, 40(5):W05113. doi:10.1029/2003WR002557.

Ye, M., Meyer, P. D. and Neuman, S. P., 2008. On Model Selection Criteria in Multimodel Analysis. Water Resources Research, 44(3): W03428. doi:10.1029/2008WR006803.

Ye, M., Pohlmann, K. F., Chapman, J. B., Pohll, G. M. and Reeves, D. M., 2010. A Model Averaging Method for Assessing Ground Water Conceptual Model Uncertainty. Groundwater, 48(5):716-728. doi:10.1111/j.1745-6584.2009.00633.x.

Table captions

Table 1. Results obtained by relying solely on two-phase data, $MSD = J/n$, and making use of two- and three-phase data: measurement error variance, $\hat{\sigma}_Y^2$, ML estimates of parameter θ_i, $\hat{\theta}_i$, and associated ML estimation error, $\hat{\sigma}_{\theta_i}^{ML}$.

Table 2. ML and sample confidence interval (CI) bounds of ML parameter estimates $\hat{\theta}_i$ (listed in Table 1) for candidate models with identifiable parameters.

Figure captions

Fig. 1. Sketch of the experimental setup; adapted from Moghadasi et al. (2016).

Fig. 2. Main steps of the procedure employed for Steady-State (SS) the (a) two- and (b) three-phase core-flooding experiments of Moghadasi et al. (2016).

Fig. 3. Two- and three-phase oil relative permeability data versus oil saturation.

Fig. 4. Schematic contour plots of J/σ_Y^2 for a two-dimensional parameter space (θ_1, θ_2) of a generic model representing (a) identifiability; (b) practical non-identifiability; and (c) structural non-identifiability of the parameters. The star represents ML estimates in the parameter space. Profile Likelihood is depicted for (d) identifiability; (e) practical non-identifiability; and (f) structural non-identifiability. Solid horizontal lines in (d)-(f) display the threshold χ_α^2 defined in (5) to identify the sample confidence intervals with significance level α.

Fig. 5. Three-phase oil relative permeability versus oil saturation. Curves represent values calculated through models M_1 - M_4 based (a) solely on information from two-phase data and (b) on information from two- and three-phase data.

Fig. 6. (a) Normalized uncertainty bounds quantified by $(\hat{\theta}_i + \hat{\sigma}_{\theta_i}^{ML})/\hat{\theta}_i$ for all ML parameter estimates $\hat{\theta}_i$ (b) Normalized local sensitivity of $Y_i = \log k_{ro,i}$ calculated at the ML estimate $\hat{\theta}_i$, for each of the oil relative permeability data available.

Fig. 7. Difference $\delta_{PL}(\theta_i) - \delta_{PL}(\hat{\theta}_i)$ (solid black curve) versus uncertain parameter (a) S_{or} of M_1; (b) S_{or} and (c) $\bar{S}_{gt}$ of M_2; (d) A and (e) B of M_3 and (f) λ and (g) β of M_4. Also depicted (*i*) χ^2_α evaluated with α = 0.317 (blue horizontal dashed lines), and α = 0.05 (green horizontal dashed lines); as well (*ii*) $\theta_{i\_U}^{ML}$ and $\theta_{i\_L}^{ML}$ evaluated with α = 0.317 (red vertical dashed lines), and α = 0.05 (red vertical continuous lines), whenever these bounds are comprised within the parameter range of variability.

Fig. 8. (a) Model selection criteria evaluated on the basis of ML calibration of models M_1-M_4. Posterior model weight/ probability evaluated considering (b) all models M_1-M_4, or (c) only models M_3-M_4 with identifiable parameters.

Fig. 9. MLBMA estimates of k_{ro} versus experimental data for *IC* = (a) *NLL*; (*b*) AIC_c; (*c*) *BIC*; and (*d*) *KIC*.

Table 1 Results obtained by relying solely on two-phase data, $MSD = J/n$, and making use of two- and three-phase data: measurement error variance, $\hat{\sigma}_Y^2$, ML estimates of parameter θ_i, $\hat{\theta}_i$, and associated ML estimation error, $\hat{\sigma}_{\theta_i}^{ML}$.

Models	*MSD*	$\hat{\sigma}_Y^2$	θ_i	$\hat{\theta}_i$	$\hat{\sigma}_{\theta_i}^{ML}$
M1 (Stone 1970)	0.047	0.037	S_{or}	0.045	0.045
M2 (Baker 1988)	0.075	0.075	S_{or}	0.11	2674
			$\overline{S}_{gt}$	1.72×10^{-4}	0.01
M3 (Du et al. 2004)	0.202	0.095	A	1.66	2.32
			B	8.78	6.64
M4 (Ranaee et al. 2015)	0.059	0.023	λ	5.44	1.95
			β	16.46	7.3

Table 2 ML and sample confidence interval (CI) bounds of ML parameter estimates $\hat{\theta}_i$ (listed in Table 1) for candidate models with identifiable parameters.

Models	θ_i	ML CI				Sample CI			
		$\alpha = 0.317$		$\alpha = 0.05$		$\alpha = 0.317$		$\alpha = 0.05$	
		$\theta_{i\_L}^{ML}$	$\theta_{i\_U}^{ML}$	$\theta_{i\_L}^{ML}$	$\theta_{i\_U}^{ML}$	$\theta_{i\_L}^{PL}$	$\theta_{i\_U}^{PL}$	$\theta_{i\_L}^{PL}$	$\theta_{i\_U}^{PL}$
M_3 (Du et al. 2004)	A	-0.66	+3.98	-2.99	+6.3	-1.62	+7.2	-4.89	+17.6
	B	+2.14	+15.43	-4.5	+22.07	+1.23	+27	-2.65	+64
M_4 (Ranaee et al. 2015)	λ	+3.49	+7.4	+1.53	+9.34	+0.99	+14.5	-1.23	+16.05
	β	+9.16	+23.76	+1.85	+31.07	+1.99	+54	-1.2	+55

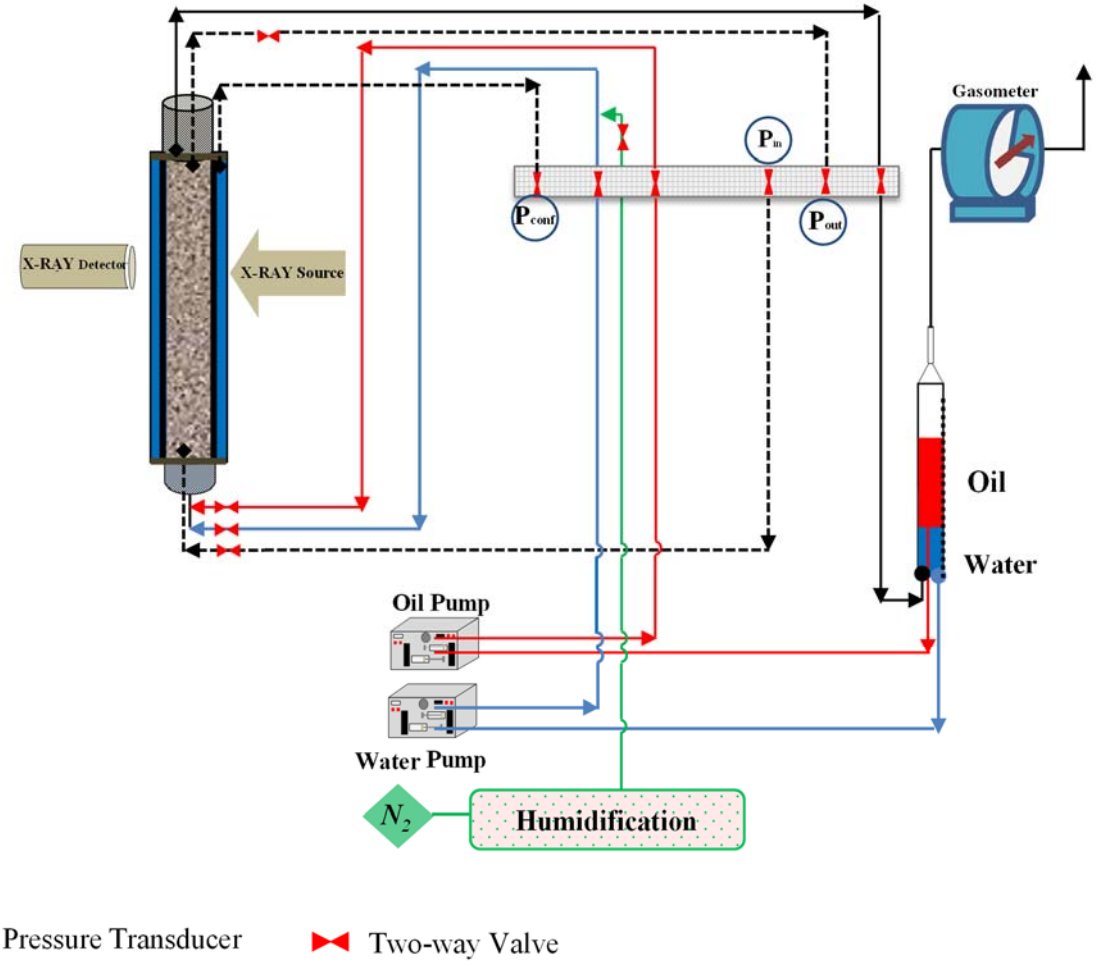

Fig. 1. Sketch of the experimental setup; adapted from Moghadasi et al. (2016).

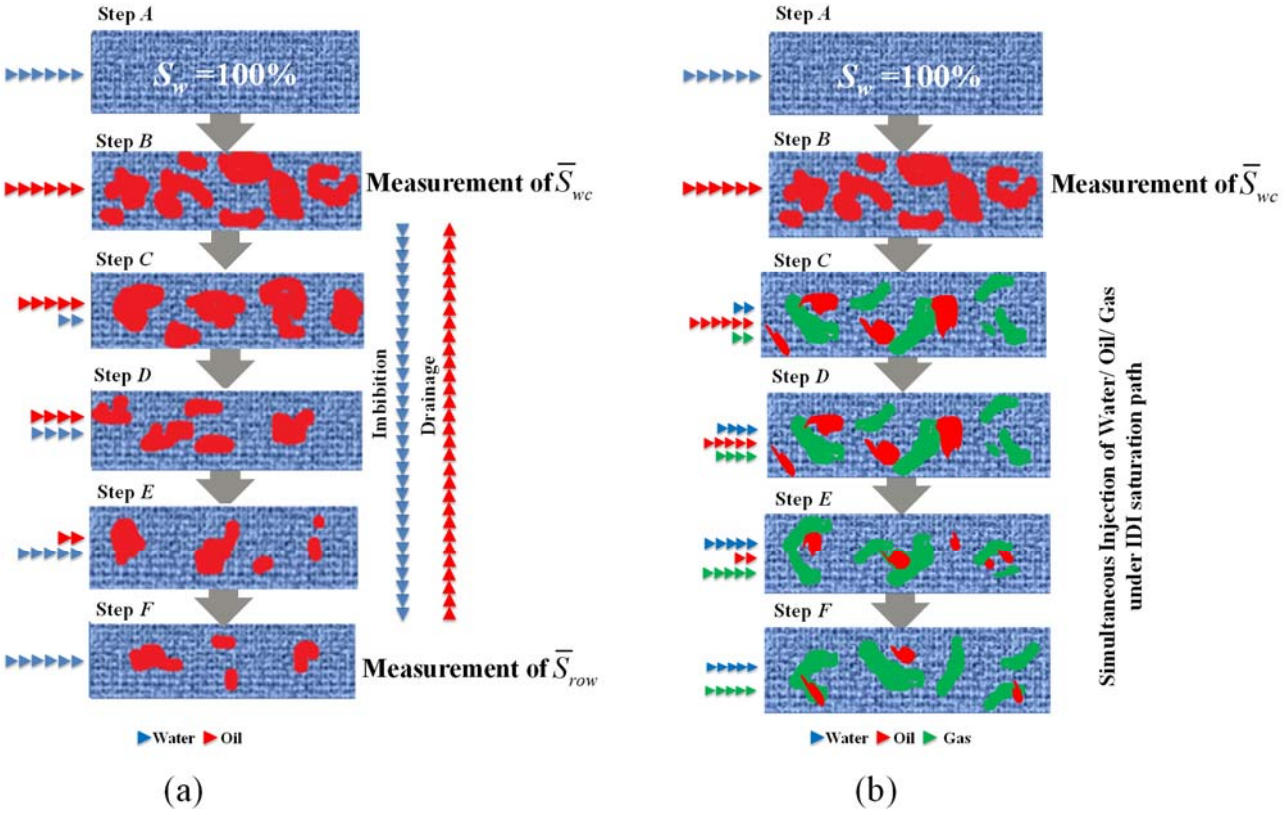

Fig. 2. Main steps of the procedure employed for Steady-State (SS) the (a) two- and (b) three-phase core-flooding experiments of Moghadasi et al. (2016).

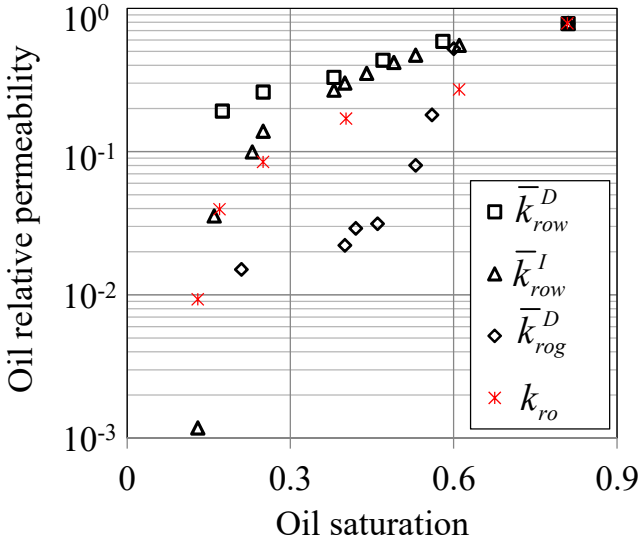

Fig. 3. Two- and three-phase oil relative permeability data versus oil saturation.

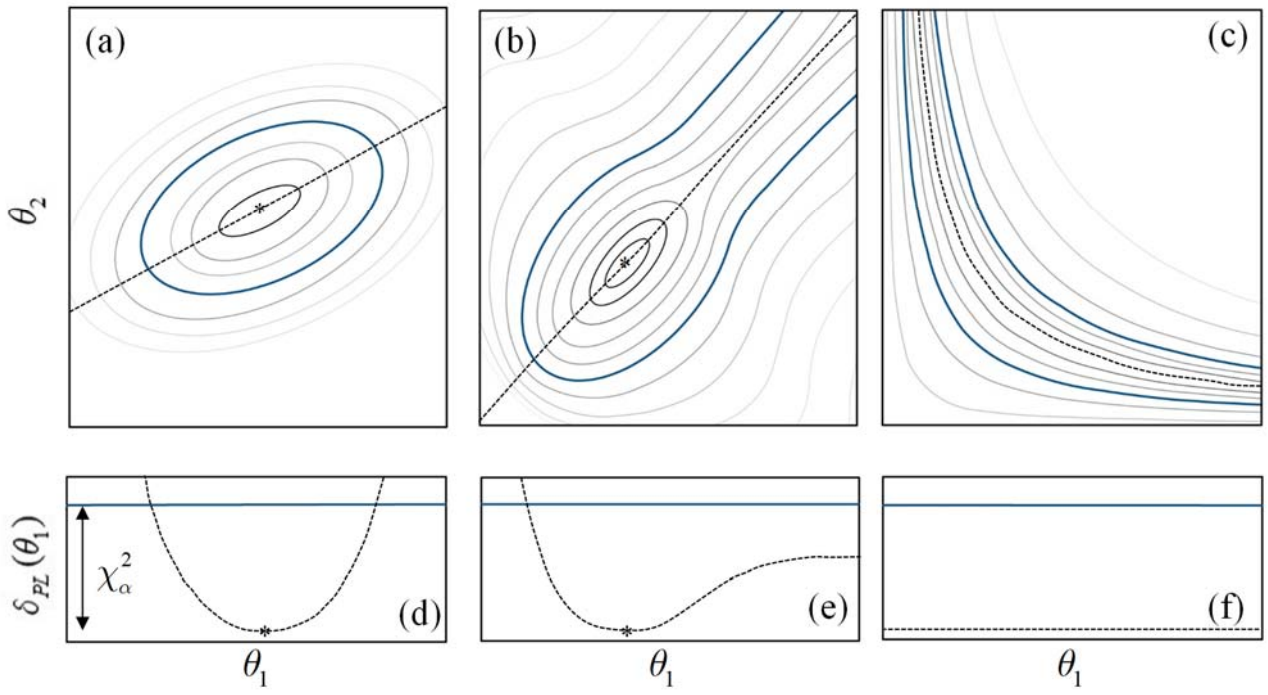

Fig. 4. Schematic contour plots of J/σ_Y^2 for a two-dimensional parameter space (θ_1, θ_2) of a generic model representing (a) identifiability; (b) practical non-identifiability; and (c) structural non-identifiability of the parameters. The star represents ML estimates in the parameter space. Profile Likelihood is depicted for (d) identifiability; (e) practical non-identifiability; and (f) structural non-identifiability. Solid horizontal lines in (d)-(f) display the threshold χ^2_α defined in (5) to identify the sample confidence intervals with significance level α.

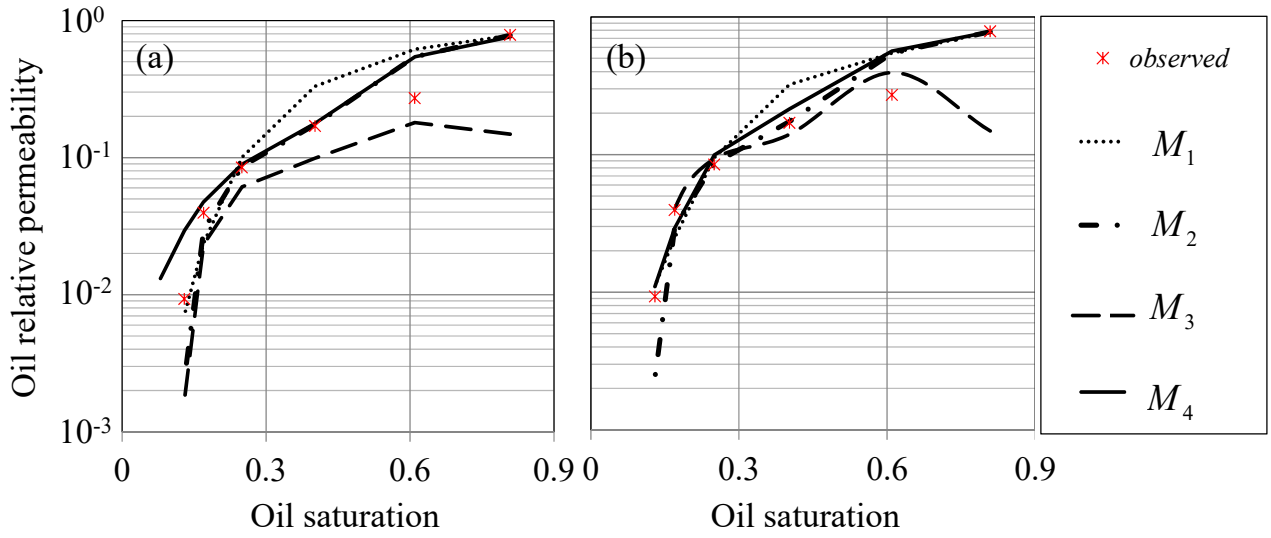

Fig. 5. Three-phase oil relative permeability versus oil saturation. Curves represent values calculated through models *M1* - *M4* based (a) solely on information from two-phase data and (b) on information from two- and three-phase data.

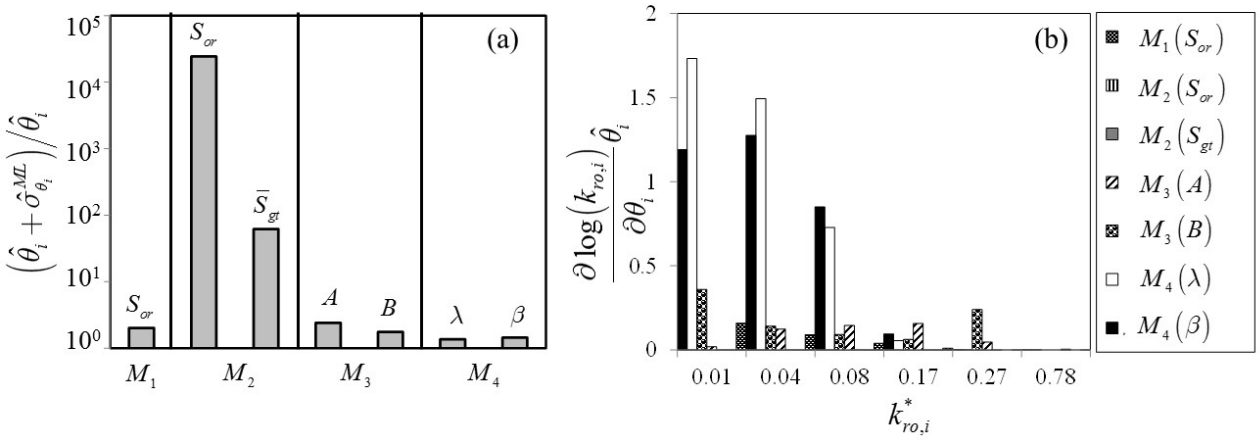

Fig. 6. (a) Normalized uncertainty bounds quantified by $(\hat{\theta}_i + \hat{\sigma}^{ML}_{\theta_i})/\hat{\theta}_i$ for all ML parameter estimates $\hat{\theta}_i$ (b) Normalized local sensitivity of $Y_i = \log k_{ro,i}$ calculated at the ML estimate $\hat{\theta}_i$, for each of the oil relative permeability data available.

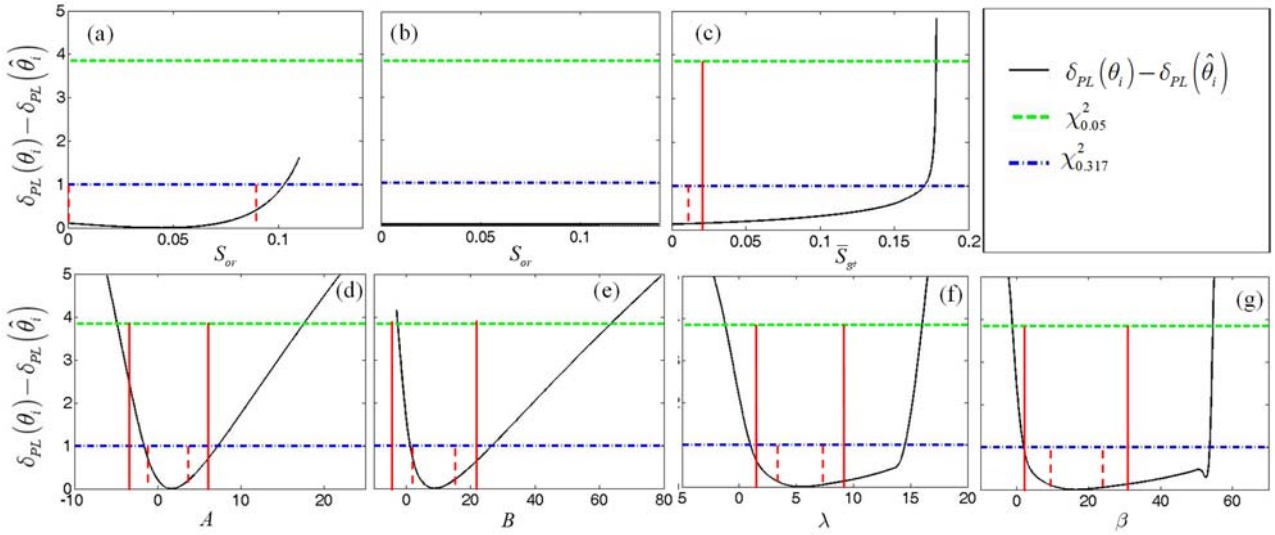

Fig. 7. Difference $\delta_{PL}(\theta_i)-\delta_{PL}(\hat{\theta}_i)$ (solid black curve) versus uncertain parameter (a) S_{or} of M_1; (b) S_{or} and (c) $\bar{S}_{gt}$ of M_2; (d) A and (e) B of M_3 and (f) λ and (g) β of M_4. Also depicted (*i*) χ^2_α evaluated with α = 0.317 (blue horizontal dashed lines), and α = 0.05 (green horizontal dashed lines); as well (*ii*) $\theta^{ML}_{i\_U}$ and $\theta^{ML}_{i\_L}$ evaluated with α = 0.317 (red vertical dashed lines), and α = 0.05 (red vertical continuous lines), whenever these bounds are comprised within the parameter range of variability.

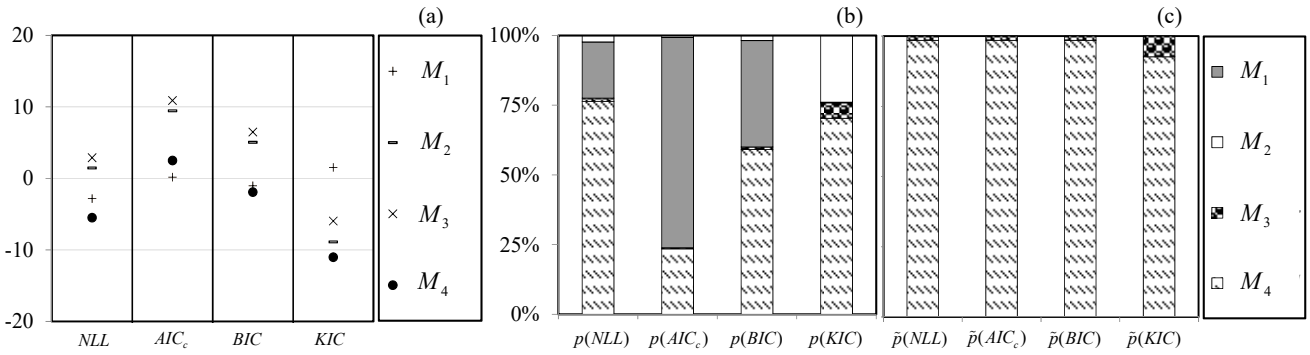

Fig. 8. (a) Model selection criteria evaluated on the basis of ML calibration of models M_1-M_4. Posterior model weight/ probability evaluated considering (b) all models M_1-M_4, or (c) only models M_3-M_4 with identifiable parameters.

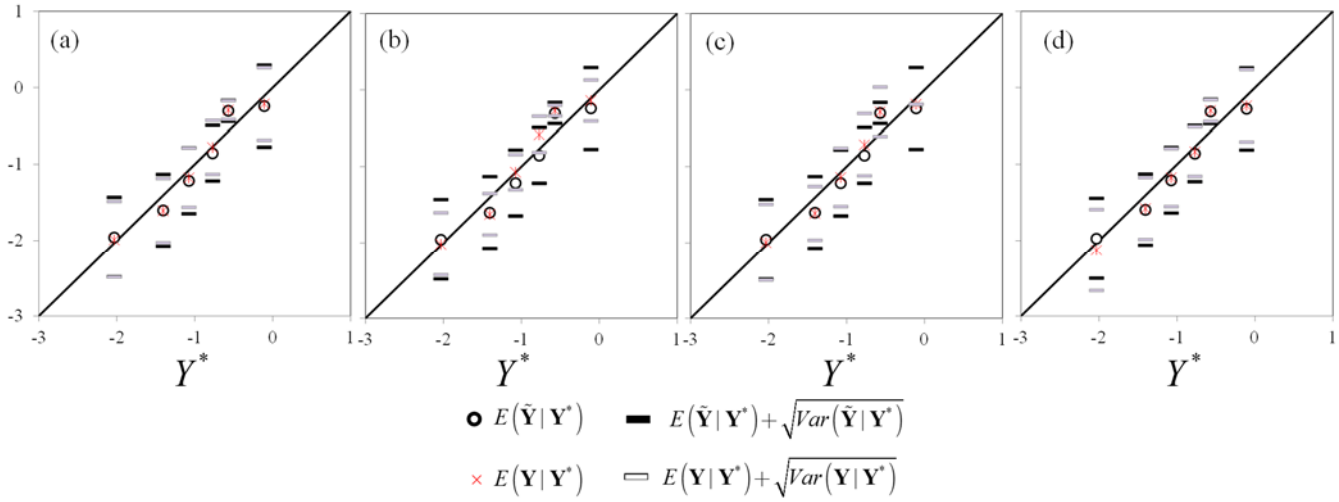

Fig. 9. MLBMA estimates of k_{ro} versus experimental data for *IC* = (a) *NLL*; (*b*) AIC_c; (*c*) *BIC*; and (*d*) *KIC*.